

# Hadronization processes in neutrino interactions

Tepei Katori and Shivesh Mandalia

*School of Physics and Astronomy, Queen Mary University of London, London E1 4NS, UK*

**Abstract.** Next generation neutrino oscillation experiments utilize details of hadronic final states to improve the precision of neutrino interaction measurements. The hadronic system was often neglected or poorly modelled in the past, but they have significant effects on high precision neutrino oscillation and cross-section measurements. Among the physics of hadronic systems in neutrino interactions, the hadronization model controls multiplicities and kinematics of final state hadrons from the primary interaction vertex. For relatively high invariant mass events, many neutrino experiments rely on the PYTHIA program. Here, we show a possible improvement of this process in neutrino event generators, by utilizing expertise from the HERMES experiment. Finally, we estimate the impact on the systematics of hadronization models for neutrino mass hierarchy analysis using atmospheric neutrinos such as the PINGU experiment.

**Keywords:** neutrino, cross section, hadronization, PYTHIA, GENIE

**PACS:** 11.80.Cr,13.15.+g,14.60.Lm,14.60.Pq,25.30.Fj,25.30.Pt,95.85.Ry

## PYTHIA, the standard hadronization model

The PYTHIA Monte Carlo (MC) generator [1, 2] is regarded as one of the standard tools for hadronization. Fragmentation in PYTHIA is described by the Lund string fragmentation model, which is a model based on the dynamics of one-dimensional relativistic strings that are stretched between coloured partons. These strings represent the colour flux and in particular, are subject to a linear confinement potential. The hadronization process is described by break-ups in the strings through the production of a new quark-antiquark pairs. An iterative approach is used to perform the fragmentation as each break up is causally disconnected. The production rate of the created  $q\bar{q}$  pair is determined using the tunnelling mechanism, which leads to a Gaussian spectrum of the transverse momentum,  $p_{\perp}^2 (= p_x^2 + p_y^2)$ , for the produced hadron. The fraction of  $E + p_z$  taken by the produced hadron is given by the variable  $z$ , defined by the hadron energy  $E$  and energy transfer  $\nu$  ( $z = E/\nu$ ). An associated fragmentation function  $f(z)$  gives the probability that a given  $z$  is chosen. The simplified Lund symmetric fragmentation function is given by,

$$f(z) \propto z^{-1}(1-z)^a \cdot \exp(-bm_{\perp}^2/z). \quad (1)$$

Here,  $m_{\perp}^2$  is the transverse mass of the hadron ( $m_{\perp}^2 \equiv m^2 + p_{\perp}^2$ ). The Gaussian term describes quantum tunnelling in the transverse direction, and tunable ‘‘Lund  $a$ ’’ and ‘‘Lund  $b$ ’’ parameters describe the longitudinal distribution of energy. Thus, these two parameters mainly decide how to distribute available energy to the produced hadrons. Frankly, larger Lund  $a$  and smaller Lund  $b$  parameters shift the fragmentation function to a lower  $z$  region. The values of these parameters are obtained from the shapes of the measured fragmentation functions, and default values of Lund  $a$  and Lund  $b$  in PYTHIA6.3 are 0.3 and 0.58 GeV/c<sup>2</sup> respectively.

## AGKY model

GENIE is a ROOT-based neutrino interaction MC generator [3]. In the few-GeV energy region which are particularly important in oscillation experiments. In GENIE, DIS interactions employ a new hadronization model called the AGKY model [4, 5].

The AGKY model is split into two parts. At lower energy regions where PYTHIA hadronization models deteriorate, a phenomenological description based on the Koba-Nielson-Olesen (KNO) scaling law is used [6]. The KNO scaling law relates the dispersion of hadron multiplicity at different invariant masses with a universal scaling function  $f(n/\langle n \rangle)$ ,

$$\langle n \rangle \times P(n) = f(n/\langle n \rangle) \quad (2)$$

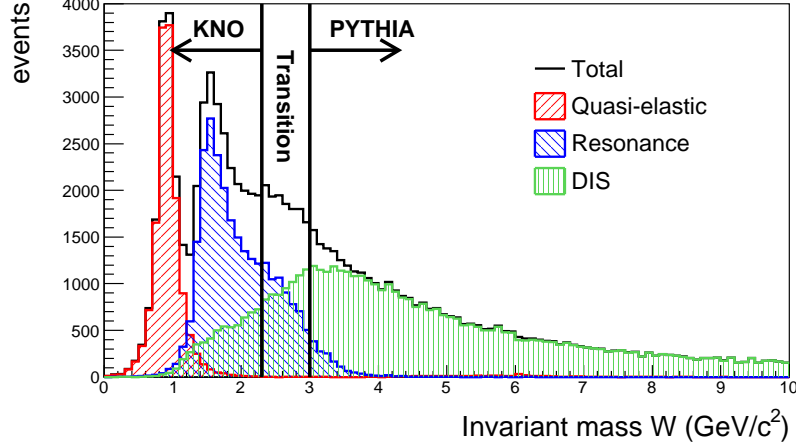


**FIGURE 1.** (color online)  $W$  distribution of  $\nu_\mu$ -water target interaction in GENIE. For the flux, we use an atmospheric  $\nu_\mu$  neutrino spectrum. Left red hatched region is quasi-elastic scattering, middle hatched region is resonance interactions, and right green hatched region is from DIS. The  $W$  distribution can be splitted to three regions, KNO scaling-based model only region, PYTHIA only region, and the transition region.

where  $\langle n \rangle$  is the averaged hadron multiplicity and  $P(n)$  is the probability of generating  $n$  hadrons. The scaling function is parametrised by the Levy function,  $L(z, c) = 2e^{-c}c^{cz+1}/\Gamma(cz+1)$  with  $z = n/\langle n \rangle$ , and an input parameter  $c$ . The input parameter is used to tune the function so it agrees with data, which is mainly taken from the Fermilab 15-foot bubble chamber [7].

At higher energy regions the AGKY model gradually transitions from the KNO scaling-based model to PYTHIA discussed previously. A transition window based on the value of the invariant hadronic mass  $W$  is used, over which the fraction of events hadronized using the PYTHIA(KNO) model increases(decreases) linearly. The default values used in the AGKY model are

- $W < 2.3 \text{ GeV}/c^2$ , KNO scaling-based model only region,
- $2.3 \text{ GeV}/c^2 < W < 3.0 \text{ GeV}/c^2$ , transition region, and
- $3.0 \text{ GeV}/c^2 < W$ , PYTHIA only region.

Figure 1 graphically shows this situation. This is the  $W$  distribution for  $\nu_\mu$ -water interactions simulated with GENIE. Here, we used a simple formula to model the atmospheric  $\nu_\mu$  neutrino spectrum [8, 9], described later. As you can see, the  $W$ -distribution in this energy region can be split into three main interaction modes, quasi-elastic (red hatched, left peak), resonance (blue hatched, middle), and DIS (green hatched, right). The AGKY model is applied to DIS interactions. Also note DIS is extended to low  $W$  region to describe non-resonance interactions in resonance region.

All studies in this paper use GENIE version 2.8.0, also figures 2, 3, 4, 5, and 6 are generated by the hadronization validation tool in GENIE.

## HERMES experiment

HERMES is a fixed target experiment at DESY [10]. The ring stores 27.6 GeV electrons or positrons, and collisions take place in the HERMES gas-jet target.

The HERMES experiment has a long history of tuning PYTHIA for their purposes. The main motivation of this is because the default PYTHIA parameters are tuned to higher energy experiments and are not quite suitable for HERMES. Since modern neutrino oscillation experiments are also lower energy (1-10 GeV) compared with collider experiments, it is interesting to test the PYTHIA developed in the HERMES experiment within GENIE. There are various tuning methods applied in PYTHIA and among them, we are most interested in the adjustment in the

fragmentation model made by tuning PYTHIA parameters. Parameter sets developed by HERMES collaborators are available elsewhere (for example, Ref. [11, 12, 13, 14]). In this article, we focus on one of parameter sets called “Lund-scan” [13], which we found had the best agreement with neutrino hadron production data. More specifically, Lund-scan is based on modifications of the following parameters from default PYTHIA values,

- PARJ(1)** = 0.02, di-quark suppression,
- PARJ(2)** = 0.25, strange quark suppression,
- PARJ(11)** = 0.51, light vector meson suppression,
- PARJ(12)** = 0.57, strange vector meson suppression,
- PARJ(21)** = 0.42, width of Gaussian  $p_{\perp}$  distribution,
- PARJ(33)** = 0.47, string breaking mass cutoff,
- PARJ(41)** = 0.68, Lund  $a$  parameter,
- PARJ(42)** = 0.35, Lund  $b$  parameter, and
- PARJ(45)** = 0.74, adjustment of Lund-string  $a$  parameter for di-quark.

Note we only tested PYTHIA parameters which are publicly available, however, HERMES also made modifications to the source code of PYTHIA itself. Therefore, in this paper we are not testing with the exact hadronization model used in the HERMES experiment. Also note GENIE version 2.8.0 tunes four PYTHIA parameters by default (PARJ(2)=0.21, PARJ(21)=0.44, PARJ(23) = 0.01, PARJ(33) = 0.20), therefore “default GENIE” quoted in this paper is not GENIE with default PYTHIA 6.3. However, the difference of predictions by default GENIE and GENIE with default PYTHIA is very small.

### Averaged charged hadron multiplicity

Averaged charged hadron multiplicity data is fundamental in the development of hadronization models. They describe the average number of charged hadrons, mainly  $\pi^+$  and  $\pi^-$ , measured with a function of invariant mass  $W$ . Neutrino hadronization models are largely guided by such data from bubble chamber experiments. Recently, Kuzmin and Naumov performed detailed surveys of neutrino bubble chamber data, and chose the best sets of data to tune their model [16]. It is shown that all modern neutrino interaction generators, such as GENIE [3], NuWro [17], and

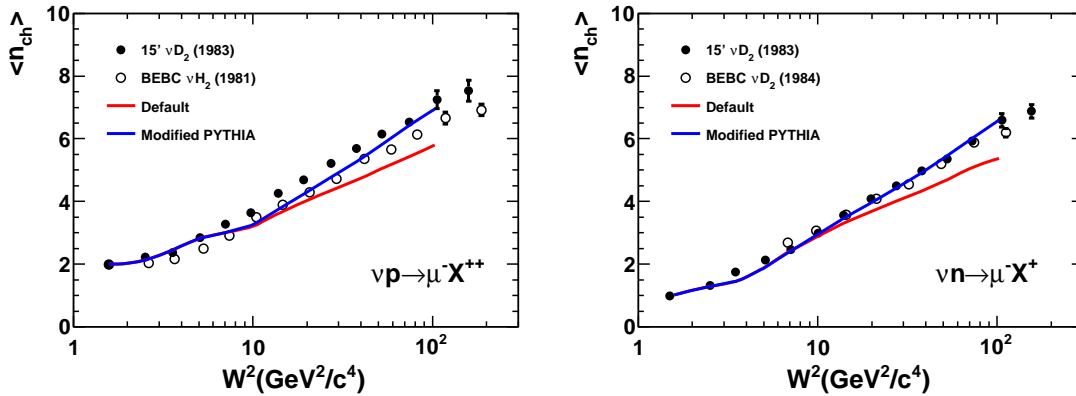


**FIGURE 2.** (color online) Averaged charged hadron multiplicity plot. Here, two predictions from GENIE are compared with bubble chamber  $\nu_{\mu} - p$  and  $\nu_{\mu} - n$  hadron production data [7, 15].

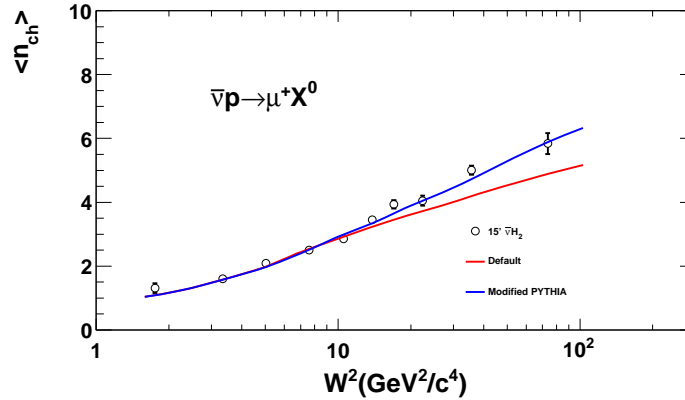


**FIGURE 3.** (color online) Averaged charged hadron multiplicity plot. Here, two predictions from GENIE are compared with bubble chamber  $\bar{\nu}_\mu - p$  hadron production data [23].

GiBUU [18], all appear to underestimate averaged charged hadron multiplicity<sup>1</sup>.

This problem largely originates from the PYTHIA fragmentation model, because as mentioned in the previous section, the default PYTHIA parameters are tuned to higher energy experiments. Both GENIE and NuWro [21] tuned these PYTHIA parameters to improve the agreement with data but the effect is marginal. Note NuWro and GiBUU use their own models for fragmentation, and only later processes are based on PYTHIA.

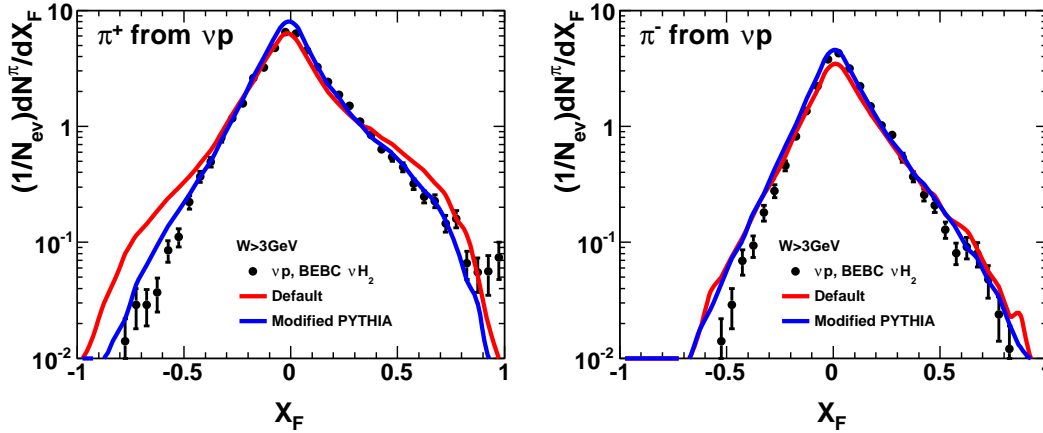
Fig. 2 shows the data-MC comparison of the averaged charged hadron multiplicity in  $\nu_\mu - p$  and  $\nu_\mu - n$  interactions. Here, the two curves represent predictions from default GENIE and GENIE with a PYTHIA modified using parameter sets described in the previous section [13]. Note, GENIE uses the AGKY model where the  $W < 2.3 \text{ GeV}/c^2$  range hadronized using the KNO scaling-based model, so these two curves should be identical at  $W < 2.3 \text{ GeV}/c^2$ . As you can see, the HERMES tune describes the data better. Here, two data sets from the Fermilab bubble chamber and BEBC agree in  $\nu_\mu - n$  interactions (both deuterium targets) but not in  $\nu_\mu - p$  data (hydrogen and deuterium target), suggesting the conflict of data we see in Fig. 2 is due to nuclear effects in deuterium [4, 5, 16, 22]. Despite with the conflict of data set, the HERMES parameterization in general increases the averaged charged hadron multiplicity, which improves the agreement with averaged charged hadron multiplicity data from neutrino bubble chamber experiments.

Fig. 3 is the same plot for  $\bar{\nu}_\mu - p$  interactions. Again, the agreement with the data is better for GENIE with the modified PYTHIA. Therefore, new parameter set works better for both neutrino and antineutrino interactions.

The main effect of this new parameterization originates from the increase of the Lund  $a$  parameter (Eq. 1). This increases averaged charged hadron multiplicity and thus it agrees better with data. In the higher energy experiments that PYTHIA is designed for, high order QCD effects cause additional low energy parton emissions. This causes hadrons to be produced with a broader spectrum in  $z$ . For the neutrino experiments we are concerned with, these effects are negligible, so we shift the peak of the fragmentation function to a lower  $z$  value by increasing the Lund  $a$  parameter [12].

In fact, all parameterization schemes from HERMES we checked have a high Lund  $a$  parameter, and many have even higher than what we are using here. However, these higher Lund  $a$  parameter models tend to overestimate hadron multiplicities compared to neutrino hadron production data from bubble chamber experiments and as a result the data-MC agreement becomes worse. The neutrino hadronization data prefer a relatively smaller Lund  $a$  parameter than HERMES, yet bigger than the default PYTHIA choice, and this is the main reason why we chose this specific parameterization scheme in this paper.

<sup>1</sup> It is also shown that the NEUT neutrino interaction generator [19], which is used by T2K and Super-Kamiokande, also underestimates averaged charged hadron multiplicity [20].



**FIGURE 4.** (color online)  $x_F$  distribution for  $\pi^+$  and  $\pi^-$  from  $\nu_\mu - p$  interactions [24]. Again, modified PYTHIA has a better agreement with data.

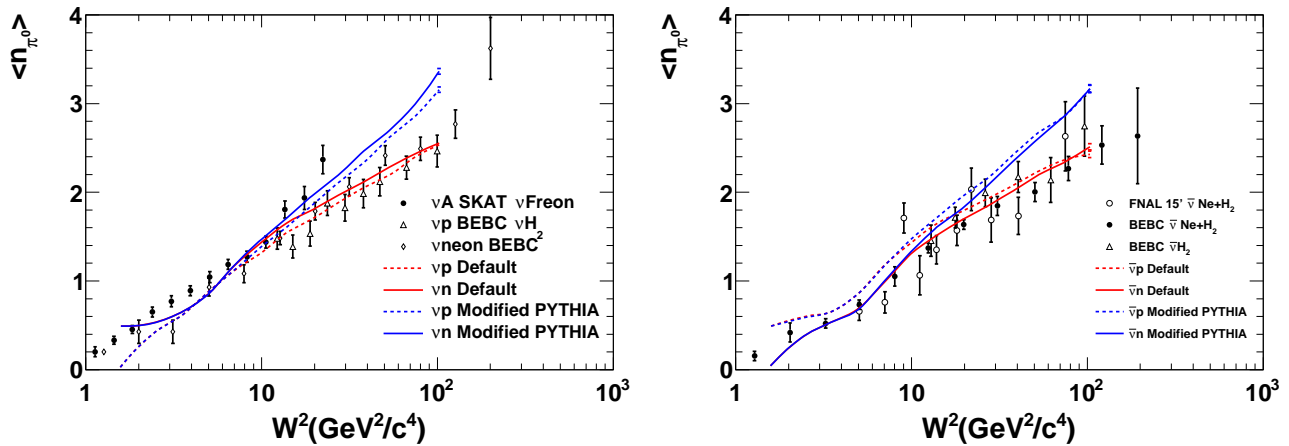


**FIGURE 5.** (color online) Averaged neutral pion multiplicity plot. Here, two predictions from GENIE are compared with bubble chamber  $\nu_\mu - p$ ,  $\nu_\mu - n$ ,  $\bar{\nu}_\mu - p$ , and  $\bar{\nu}_\mu - n$   $\pi^0$  production data [25, 26, 27, 28].

### $x_F$ distribution

Feynman  $x$ ,  $x_F$ , is the fraction of longitudinal momentum available for a hadron, defined in the hadronic center mass system, *i.e.*,  $x_F = \frac{P_L^*}{P_{Lmax}^*} \sim \frac{2P_L^*}{W}$ , here asterisks stand for the hadron c.m.s. Fig. 4 shows the data-MC comparison. The agreement of modified PYTHIA with bubble chamber is excellent for both  $\pi^+$  and  $\pi^-$  data. Therefore the tuning we applied is valid not only for averaged charged hadrons, but also valid for positive and negative hadrons separately.

### Averaged neutral pion multiplicity

In Figure 5, predictions are compared with the averaged  $\pi^0$  multiplicity. Here the data from  $\nu_\mu$  and  $\bar{\nu}_\mu$  interactions are from various targets [25, 26, 27, 28] Although the data here have larger errors, now the default GENIE has a better

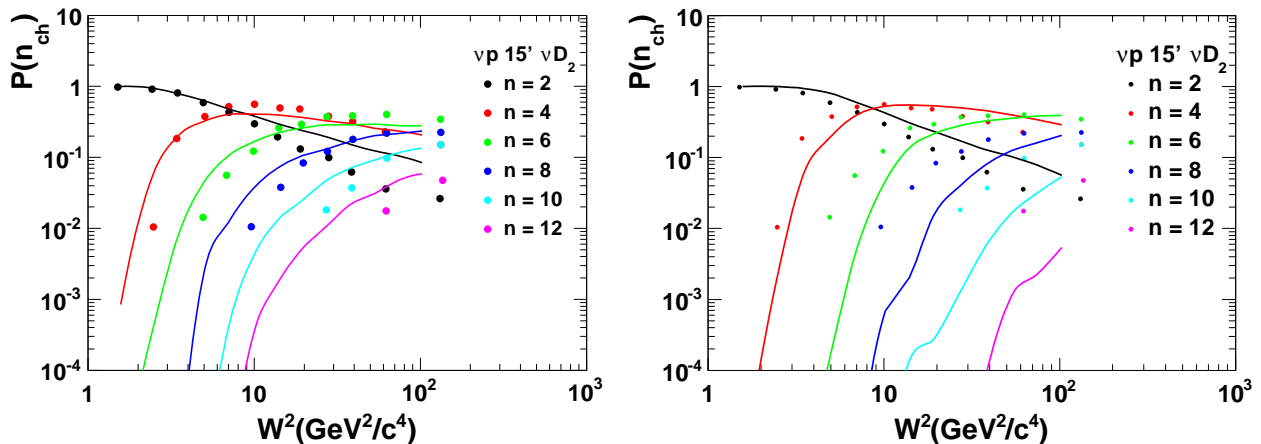


**FIGURE 6.** (color online) Topological cross sections of charged hadrons for  $\nu_\mu - p$  interaction. In both figures, data points are from Ref. [7]. In the left plot, PYTHIA is turned off and data is compared with GENIE with only the KNO scaling-based hadronization model. On the other hand, in the right figure, PYTHIA is extend all way to  $W=1.3 \text{ GeV}/c^2$  so that hadronization is almost solely handled by PYTHIA.

agreement with the data. The ratio of number of produced charged pions and neutral pions is strongly tied due to isospin symmetry, *i.e.*  $N(\pi^+) + N(\pi^-) : N(\pi^0) = 2 : 1$ . This means, if we increase the charged hadron multiplicity in the hadronization model, the model will also have a higher multiplicities of neutral pions. The charged pion and neutral pion multiplicity ratio is 2:1 in BEBC neon target bubble chamber data [25], however, it is not easy to achieve good agreements with both charged hadron and neutral pion multiplicities including other data sets by tuning PYTHIA. On the other hand, PYTHIA shows excellent agreements in both charged and neutron pion fragmentation functions with HERMES data [10, 29].

## Topological cross sections

In the low  $W$  region, PYTHIA does not predict the multiplicity properly. In GENIE, the AGKY model uses a phenomenological approach based on KNO scaling [6], where dispersion is assumed to follow a scaling law as data suggest. Thus, by definition, the AGKY model has good data-MC agreement for the dispersion of the multiplicity in the low  $W$  region. This is not the case in PYTHIA, where physics is simulated from a more first principles approach, which is based on quark-diquark fragmentation. By tuning PYTHIA parameters, data-MC agreement of the averaged charged hadron multiplicity can be improved, but it is not as easy to correct the dispersion.

Figure 6 shows data-MC comparisons of the topological cross sections of charged hadrons, that is, the fraction of final particle topologies of a given interaction as function of invariant mass. In both plots, the GENIE predictions are compared with  $\nu_\mu - p$  data [7]. In the left plot, GENIE hadronization model is solely carried out by the KNO scaling-based model. Since the KNO scaling-based approach reproduces the dispersion data by definition, GENIE can reproduce the data at large multiplicities, such as  $n=6$ ,  $n=8$ , etc.

On the other hand, in the right plot, the GENIE hadronization model solely depends on PYTHIA.<sup>2</sup> In this case, we see PYTHIA has problems reproducing large hadron multiplicity events. The combination of KNO scaling-based model and PYTHIA cannot make a smooth curve in the large multiplicity limit. We also checked the KNO scaling law in PYTHIA. PYTHIA also satisfies the KNO scaling law, however, the width of multiplicity is much narrower than the distribution extracted from the data. Thus, we conclude that the dispersion of charged hadron multiplicity produced by PYTHIA is narrower than the data, and this makes harder to produce large numbers of hadrons when averaged hadron

<sup>2</sup> Note in GENIE there is a limitation to how far one can extend PYTHIA to low invariant masses, and thus below  $1.4 \text{ GeV}/c^2$  there are contribution from the KNO scaling-based model

multiplicity is small. Therefore, it is also important to tune PYTHIA to reproduce the charged hadron multiplicity dispersion data, not just the averaged charged hadron multiplicity.

High resolution liquid argon time projection chamber (LArTPC) experiments, such as MicroBooNE [30], are in a good position to identify high multiplicity hadron events. These data may offer the opportunity to test neutrino hadronization processes. However, to test hadronization models with hadron data from heavy nuclear targets such as argon, it is also necessary to have a good model for primary interactions [31, 32] and nuclear effects [33]. The main focus of this CETUP 2014 neutrino interaction workshop was inelastic interaction processes, where both primary interactions and nuclear effects play significant roles and currently disagreements between data and predictions are not well understood [31, 32, 34]. Therefore, it is challenging to develop a hadronization model solely from neutrino experimental data, and input from other fields, especially electron scattering experiments, are very important.

## Impact on hadronization models for PINGU

PINGU [35] is a low energy extension of the IceCube detector [36]. By placing optical sensors closer together compared to the original IceCube detector, PINGU is able to measure atmospheric neutrinos below 20 GeV where matter oscillations are important. Although PINGU has a significantly smaller volume coverage compared with the 1km<sup>3</sup> IceCube detector, the estimated PINGU volume coverage is still  $\sim 6$  Mton and high statistics is expected. The capability of atmospheric neutrino oscillation measurements has also been demonstrated recently [37].

The goal of PINGU is to determine the neutrino mass hierarchy (NMH) through matter oscillations. In the two-neutrino oscillation approximation, the muon neutrino oscillation probability in the normal hierarchy ( $P_{\alpha\beta}^{NH}$ ) and the muon anti-neutrino disappearance oscillation probability in the inverted hierarchy ( $\bar{P}_{\alpha\beta}^{IH}$ ) are the same ( $P_{\alpha\beta}^{NH} = \bar{P}_{\alpha\beta}^{IH}$ ,  $\bar{P}_{\alpha\beta}^{NH} = P_{\alpha\beta}^{IH}$ ) [38]. So it is also desirable to separate muon neutrinos and muon anti-neutrinos where final state leptons are indistinguishable by Cherenkov detectors such as PINGU.

Recently, Ribordy and Smirnov pointed out that the charge separation, through the precise measurement of inelasticity distributions, improves the PINGU and ORCA [39] NMH sensitivity [38]. The same story may be applied to Hyper-Kamiokande [40] and LBNF [41]. Since inelasticity measurements rely on the energy deposits of hadronic showers, it is interesting to check the impact of different hadronization models in this situation.

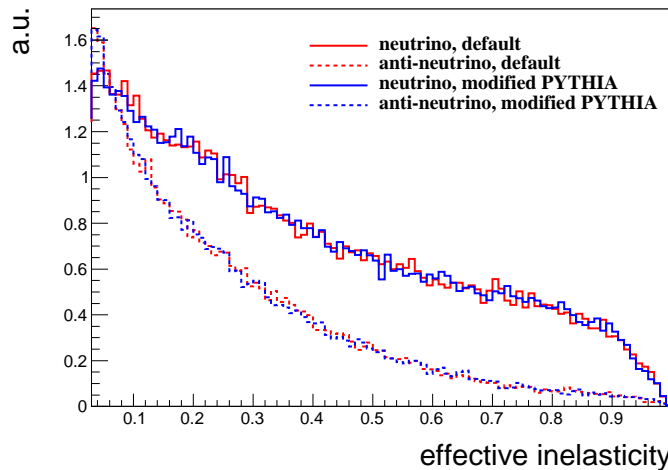


**FIGURE 7.** (color online) Effective inelasticity distribution with atmospheric neutrino spectrum. Here, all histograms are arbitrarily normalized. Solid histograms are muon neutrino distributions, and dashed histograms are muon anti-neutrino distributions. Red histograms are from GENIE with the default hadronization model, and blue histograms are from GENIE with the modified hadronization model discussed in this paper.

For this purpose, we estimated the impact of hadronization models on the effective inelasticity. We define the effective inelasticity from the visible hadron shower energy.

$$E_h^{vis} = \sum_{E_h^i > E_{th}^i} T_h^i + \sum E_\gamma^i. \quad (3)$$

Here, the first term is the sum of kinetic energies of charged hadrons above the Cherenkov threshold, the assumption here is that the hadrons above the Cherenkov threshold are visible and so we take into account their kinetic energies. The second term is the sum of all the final state photons, including the decays of neutral mesons. Thus, the visible hadron energy corresponds to the energy deposit from the hadronic system to the perfect photon detector, where inefficiency is only from neutrons or hadrons below the Cherenkov threshold. Then, the effective inelasticity,  $y^{eff}$ , is defined by,

$$y^{eff} = \frac{E_h^{vis}}{E_h^{vis} + E_\mu}. \quad (4)$$

Here  $E_\mu$  is the muon (anti-muon) energy.

To simulate effective inelasticity on a water target, we modelled the atmospheric neutrino flux with a simple formula ( $\sim a + b \cdot E^{-c}$ , where  $c \sim 2.8$ ) which reproduces the typical energy spectrum of atmospheric neutrinos [8, 9]. Then we simulate neutrino interaction from 2 to 30 GeV where is the important region for NMH analysis.

Figure 7 shows the result. The  $y^{eff}$  distributions for neutrino and anti-neutrino interactions are well separated, however,  $y^{eff}$  distributions based on different hadronization models are very similar. This result can be understood from simulated  $W$  distribution in PINGU (Fig. 1). The important region for PINGU is still dominated by low  $W$  interactions, where PYTHIA hadronization processes have a minor role. This indicates alternations of the hadronization model only provide minor changes to the systematics of the PINGU inelasticity measurement, however, details have yet to be tested with a full PINGU detector simulation.

## Conclusion

In this article, we studied neutrino hadronization processes in GENIE. Our main focus is to improve the averaged charged hadron multiplicity, and it is shown that suitable parameterization developed by the HERMES collaboration dramatically improves the data-MC agreement with neutrino bubble chamber data. However, this tuning may make the  $\pi^0$  multiplicity agreement slightly worse. Also dispersion of hadron multiplicity is still not under control. Near future LArTPC experiment, such as MicroBooNE, could test the hadronization models by measuring high hadron multiplicity events.

In both J-PARC neutrino beam [42] and NuMI [43], flux peaks are tuned to quasi-elastic or resonance dominant regions where oscillation effects are bigger. However, off-axis neutrino beams made from wideband decay-in-flight neutrino beams have long high-energy tails, and the contribution from large  $W$  interaction is always present. For example, multi-pion production processes contribute significant amounts in single pion production measurements at T2K [20]. Therefore correct modelling of hadronization process is an important subject for current and future long baseline oscillation experiments [35, 39, 40, 41, 43, 44].

Finally, we tested different hadronization models with a modelled atmospheric neutrino flux. It turns out the difference in the inelasticity distributions is small, suggesting the hadronization processes only plays a minor role in the systematics for NMH analysis at atmospheric neutrino oscillation experiments, such as PINGU and Hyper-Kamiokande.

## ACKNOWLEDGMENTS

TK thanks Ulrich Mosel for introducing this subject to us. We thank Elke Aschenauer and Josh Rubin for useful information about the HERMES experiment. We also appreciate the various help given to us by GENIE collaborators on this analysis. Finally, TK would like to thank the organizer of CETUP\* (Center for Theoretical Underground Physics and Related Areas) for the hospitality during my stay at Deadwood, SD, to complete this work.



## REFERENCES

1. T. Sjostrand, S. Mrenna, and P. Z. Skands, *JHEP* **0605**, 026 (2006), hep-ph/0603175.
2. T. Sjostrand, S. Mrenna, and P. Z. Skands, *Comput.Phys.Commun.* **178**, 852–867 (2008), 0710.3820.
3. C. Andreopoulos, A. Bell, D. Bhattacharya, F. Cavanna, J. Dobson, et al., *Nucl.Instrum.Meth.* **A614**, 87–104 (2010), 0905.2517.
4. T. Yang, C. Andreopoulos, H. Gallagher, K. Hoffmann, and P. Kehayias, *Eur.Phys.J.* **C63**, 1–10 (2009), 0904.4043.
5. T. Yang (2009), FERMILAB-THESIS-2009-04.
6. Z. Koba, H. B. Nielsen, and P. Olesen, *Nucl.Phys.* **B40**, 317–334 (1972).
7. D. Zieminska, S. Kunori, C. Chang, G. Snow, D. Son, et al., *Phys.Rev.* **D27**, 47–57 (1983).
8. M. Honda, T. Kajita, K. Kasahara, and S. Midorikawa, *Phys.Rev.* **D83**, 123001 (2011), 1102.2688.
9. M. Honda, T. Kajita, K. Kasahara, S. Midorikawa, and T. Sanuki, *Phys.Rev.* **D75**, 043006 (2007), astro-ph/0611418.
10. A. Airapetian, et al., *Phys.Rev.* **D87**, 074029 (2013), 1212.5407.
11. F. M. Menden (2001), DESY-THESIS-2001-060.
12. A. Hillenbrand (2005), DESY-THESIS-2005-035.
13. J. G. Rubin (2009), DESY-THESIS-2009-045.
14. A. Airapetian, et al., *JHEP* **1008**, 130 (2010), 1002.3921.
15. P. Allen, et al., *Nucl.Phys.* **B181**, 385 (1981).
16. K. S. Kuzmin, and V. A. Naumov, *Phys.Rev.* **C88**, 065501 (2013), 1311.4047.
17. C. Juszczak, J. A. Nowak, and J. T. Sobczyk, *Nucl.Phys.Proc.Suppl.* **159**, 211–216 (2006), hep-ph/0512365.
18. O. Buss, T. Gaitanos, K. Gallmeister, H. van Hees, M. Kaskulov, et al., *Phys.Rept.* **512**, 1–124 (2012), 1106.1344.
19. Y. Hayato, *Nucl.Phys.Proc.Suppl.* **112**, 171–176 (2002).
20. K. T. Connolly (2014), T2K-THESIS-043.
21. J. A. Nowak, *Phys.Scripta* **T127**, 70–72 (2006), hep-ph/0607081.
22. J. A. Nowak, and J. T. Sobczyk, *Acta Phys.Polon.* **B37**, 2371–2378 (2006), hep-ph/0608108.
23. M. Derrick, P. Gregory, F. LoPinto, B. Musgrave, J. Schlereth, et al., *Phys.Rev.* **D25**, 624 (1982).
24. P. Allen, et al., *Nucl.Phys.* **B214**, 369 (1983).
25. W. Wittek, et al., *Z.Phys.* **C40**, 231 (1988).
26. A. Ivanilov, V. Konyushko, V. Korablev, V. Korotkov, V. Makeev, et al., *Yad.Fiz.* **41**, 1520–1534 (1985).
27. H. Grassler, et al., *Nucl.Phys.* **B223**, 269 (1983).
28. V. Ammosov, A. Amrakhov, A. Denisov, P. Ermolov, V. Gapienko, et al., *Nuovo Cim.* **A51**, 539 (1979).
29. S. J. Joosten (2013), DESY-THESIS-2013-044.
30. G. Karagiorgi, *Phys.Procedia* **37**, 1319–1323 (2012).
31. J. G. Morfin, J. Nieves, and J. T. Sobczyk, *Adv.High Energy Phys.* **2012**, 934597 (2012), 1209.6586.
32. L. Alvarez-Ruso, Y. Hayato, and J. Nieves, *New J.Phys.* **16**, 075015 (2014), 1403.2673.
33. K. Gallmeister, and U. Mosel, *Nucl.Phys.* **A801**, 68–79 (2008), nucl-th/0701064.
34. J. Sobczyk, and J. Zmuda (2014), 1410.7788.
35. M. Aartsen, et al. (2014), 1401.2046.
36. M. Aartsen, et al., *Science* **342**, 1242856 (2013), 1311.5238.
37. M. Aartsen, et al., *Phys.Rev.Lett.* **111**, 081801 (2013), 1305.3909.
38. M. Ribordy, and A. Y. Smirnov, *Phys.Rev.* **D87**, 113007 (2013), 1303.0758.
39. A. Kouchner, *Phys.Dark Univ.* **4**, 60–74 (2014).
40. E. Kearns, et al. (2013), 1309.0184.
41. C. Adams, et al. (2013), 1307.7335.
42. K. Abe, et al., *Phys.Rev.* **D87**, 012001 (2013), 1211.0469.
43. S. Childress, and J. Strait (2013), 1304.4899.
44. K. Abe, et al., *Phys.Rev.Lett.* **112**, 061802 (2014), 1311.4750.